EurJOC
European Journal of Organic Chemistry

Full Papers
doi.org/10.1002/ejoc.202001488

Chemistry Europe
European Chemical Societies Publishing

Special Collection

Electron Donor-Acceptor Spirobi[cyclopenta[2,1-*b*:3,4-*b*′]dithiophene] Derivatives as Precursors of Electrodeposited Regioregular Thiophene-based Polymers

Daniela Minudri,[a] Simonetta Orlandi,[b] Marco Cavazzini,[b] Sergio Rossi,[c] Gabriela Marzari,[a] Pablo Cavallo,[a] Luciana Fernandez,[a] Fernando Fungo,*[a] and Gianluca Pozzi*[b]

Dedicated to Professor Franco Cozzi on the occasion of his 70th birthday.

A series of conjugation extended push-pull derivatives of 4,4′-spirobi[cyclopenta[2,1-*b*:3,4-*b*′]dithiophene] were synthesized and fully characterized, in which each perpendicularly aligned cyclopenta[2,1-*b*:3,4-*b*′]dithiophene features a pendant dicyanovinylene as an electron acceptor and a thiophene as an electron donor. The electrochemical and photophysical properties of the new molecules, which differ from each other for the presence and/or location of an additional *n*-hexyl chain on the pendant thiophene unit, were investigated, as well as their susceptibility to electrochemical polymerization. The substitution arrangement of the monomers was found to exert significant influence on the outcome of the electropolymerization process and on the optoelectronic properties and morphological film characteristics of the new regioregular materials obtained.

Introduction

The development of organic optoelectronic devices demands hole and electron-conducting materials that are able to interact efficiently with light while allowing good quality film formation.[1] In the effort to obtain this kind of organic functional materials, excellent results have been obtained by molecular engineering of spiro-configured compounds where two perpendicularly oriented molecular halves, each consisting of a polycyclic aromatic bridge linking electron donor (A) and/or acceptor (D) functionalities, are connected through a shared sp^3-hybridized atom. This general molecular scheme accommodates to compounds of very different nature, (i.e. $(A\text{-}\pi\text{-}A)_2$, $(A\text{-}\pi\text{-}D)_2$, $(D\text{-}\pi\text{-}D)_2$, but also (A-π-A)/(A′-π′-A′), (A-π-D)/(A′-π′-D′), (A-π-D)/(A-π′-D) and so on).[2,3] In any case, the orthogonal space arrangement of two spiro-linked conjugate systems with identical or different electrochemical and photophysical properties has several advantages. The electronic intramolecular interactions between the two conjugate systems are greatly reduced compared to the intermolecular interactions that would occur if the two systems were independent and free to approach each other, thus decreasing aggregation phenomena. Preventing aggregation at the molecular level improves some key-properties of the resulting materials, such as solubility, film formation ability by wet and vacuum technics, chemical and thermal stability, and ease of isotropic charge transport. On the other hand, the optoelectronic properties of solid-state systems are more defined with respect to the case of analogous non-spiro compounds, being more similar to those observed at the molecular level, and they can be finely tuned by selecting adequate A and D functionalities, together with the nature and the length of the conjugated bridges.[2,4,5] Thanks to the combination of these notable properties, spiro-configured organic functional materials, mostly derived from 9,9′-spirobifluorene, have found potential use in several optoelectronic and electronic applications, including electrochemiluminescence,[3] organic light-emitting devices (OLEDs),[6] field-effect transistors,[7] lasers,[8] and solar cells.[9–11] However, spiro compounds based on heteroaromatics are increasingly investigated in optoelectronic devices, especially as p-organic semiconductors with improved charge injecting and transporting properties.[12–15] This is well exemplified by the recent introduction of 4,4′-spirobi[cyclopenta[2,1-*b*:3,4-*b*′]dithiophene] (SCPDT) and spiro-linked fluorene-cyclopenta[2,1-*b*:3,4-*b*′]dithiophene (FDT) derivatives as molecular hole transport materials (HTM) in perovskite solar cells.[16–20] These compounds have been found to rival or even outperform the costly 2,2′,7,7′-tetrakis(*N*,*N*-di-*p*-methoxyphenylamino)-9,9′-spirobifluorene (spiro-MeOTAD), which is the benchmark HTM in solid-state dye-sensitized and perovskite solar cells.[16]

In view of the mass production of organic electronics, molecular design of organic materials for optoelectronics

[a] Dr. D. Minudri, Dr. G. Marzari, Dr. P. Cavallo, Dr. L. Fernandez, Dr. F. Fungo
IITEMA, UNRC-CONICET
Departamento de Química
Universidad Nacional de Río Cuarto
Agencia Postal 3, X5804BYA Río Cuarto, Argentina
E-mail: ffungo@exa.unrc.edu.ar
[b] Dr. S. Orlandi, Dr. M. Cavazzini, Dr. G. Pozzi
Istituto di Scienze e Tecnologie Chimiche "Giulio Natta" (SCITEC)
Consiglio Nazionale delle Ricerche (CNR)
via C. Golgi 19, 20133 Milano, Italy
E-mail: gianluca.pozzi@scitec.cnr.it
[c] Dr. S. Rossi
Dipartimento di Chimica
Università degli Studi di Milano
via C. Golgi 19, 20133 Milano, Italy

Supporting information for this article is available on the WWW under https://doi.org/10.1002/ejoc.202001488

Part of the "Franco Cozzi's 70th Birthday" Special Collection.

should envision the constraints of the techniques of deposition of organic active layers that have been developed as alternatives to expensive vacuum-based methods. Indeed, most relevant wet techniques, such as spin coating,[21] spray deposition,[22] roll-to-roll gravure printing,[23] inkjet printing,[24] brush painting,[22] and screen printing,[23] all demand organic materials with specific properties in order to ensure the deposition of active films with high morphological quality as required in the fabrication of optoelectronic devices.[25] In this respect, film formation by electropolymerization offers many advantages, despite specific difficulties found in cover homogeneously large surface areas. This one-step electrochemical method allows the simultaneous generation of electroactive polymers and their deposition on a conducting substrate, avoiding preliminary complex polymer synthesis and minimizing wastes and residues during film fabrication. Moreover, electrodeposition techniques require simple and low-cost equipment. They ensure high deposition rates at low-temperature processing and offer the opportunity to tailor the microstructure and properties of the film.[26]

Even though there are many classical examples of electrodeposited polymer films, such as those obtained from anilines, pyrroles, carbazoles, and thiophenes, examples bound to spiro-linked molecular structures are less common. Most of the spiro-molecules specifically designed to electrochemically form films are based on the 9,9′-spirobifluorene core, with applications in OLEDs,[6] electrochromic devices,[27,28] and electronic paper.[29] More recently, this research field has been expanded by introducing heteroaromatic spiro-skeleton cores with different optic and electronic characteristics.[12,30,31] Based on the stereoselective functionalization of the symmetrical SCPDT core,[32] we demonstrated the successful electropolymerizable design of electron donor-acceptor compounds with broad electronic absorption spectra in the visible region.[30] Our study proved that the choice of the well-known dimerizable triphenylamine (TPA) as the electron donor unit, in combination with the SCPDT core allows the electrochemical deposition of a photoelectroactive polymer. The obtained films retain the ability to generate photoinduced charge-separated states and to transport holes, turning this kind of material into a unique example of electropolymerizable donor-acceptor polymer with potential application in the field of organic optoelectronic devices.

From this perspective, the interest for further developments of the design of SCPDT-based monomers and for the electropolymers derived thereof is evident. We have thus pointed our attention to the possible use of thiophene as the electropolymerizable electron donor group since conjugated polymeric thiophene derivatives are among the most successful organic materials for use in optoelectronic devices.[33,34] Incorporation of cyclopentadithiophenes into the backbone of thiophene based polymers expands molecular diversity and leads to more extended conjugation and enhanced intermolecular stacking.[35,36] In addition, it is has been shown that the optical, electrochemical, solid-state packing, charge transport, among other properties of polythiophenes based films, can be affected by attaching alkyl sidechains.[37–40] Here, we focus on four structurally related push-pull SCPDT derivatives, featuring thiophene and dicyanovinylene as SCPDT-bridged pendant electron donor-and acceptor group, respectively, that differ from each other for the presence and/or location of an *n*-hexyl chain on the pendant thiophene units (Figure 1). This systematic structural variation affects the electrochemical and photophysical properties of the new molecules, their tendency to generate acceptor-donor conducting electropolymers with well-defined regioregular patterns, and the optoelectronic properties and morphological film characteristics of these materials.

Results and Discussion

Synthesis of monomers. Spiro compounds **SO4**–**SO7** (**SOs**) were prepared starting from a common precursor, namely 2,2′-dibromo-6,6′-diformyl-4,4′-spirobi[cyclopenta[2,1-*b*:3,4-*b*′]dithiophene] **1**,[32] as summarized in Scheme 1 and Scheme 2. We planned at first to functionalize the SCPDT core with two donor thiophene groups by palladium mediated C–C cross-coupling reactions, followed by the introduction of two dicyanovinylene as acceptor groups by Knoevenagel condensation with malononitrile. To this purpose, **1** was reacted with 2-thienyl boronic acid **2** under Suzuki-Miyaura cross-coupling conditions, giving the derivative **3** in good yield (Scheme 1). Condensation of dialdehyde **3** with malononitrile was accomplished in the presence of piperidine as a base in refluxing CH_2Cl_2, affording the desired compound **SO4**, which proved to be poorly soluble in common organic solvents. Following the same approach, **1** was next reacted with 5-hexylthiophene-2-boronic acid pinacol ester **4** to give the dialdehyde **5**. The attempted condensation of **4** with malononitrile under basic conditions required a large excess of malononitrile and prolonged reaction time, affording the desired product **SO5** in very low yield (less than 10%) after chromatographic purification. Better results were obtained when the **5** was reacted with malononitrile in presence of titanium tetraisopropoxide as Lewis acid in a solvent mixture dichloroethane/2-propanol 2.5/1 v/v. In this case **SO5** was smoothly obtained in 86% yield.

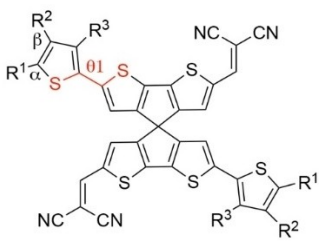

SO4 $R^1 = R^2 = R^3 = H$
SO5 $R^1 = n\text{-}C_6H_{13}$; $R^2 = R^3 = H$
SO6 $R^1 = R^2 = H$; $R^3 = n\text{-}C_6H_{13}$
SO7 $R^1 = R^3 = H$; $R^2 = n\text{-}C_6H_{13}$

Figure 1. Donor/Acceptor molecules investigated in the present work.

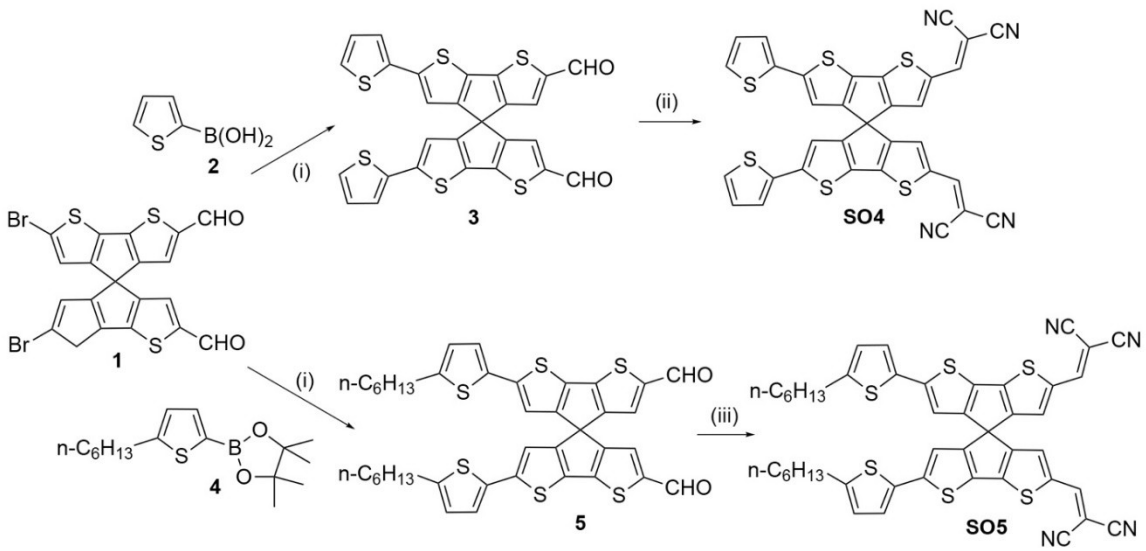

(i) $Pd(PPh_3)_4$, KF_{aq}, DME, 80°C; (ii) $CH_2(CN)_2$, Piperidine, DCM, reflux; (iii) $CH_2(CN)_2$, $Ti(OiPr)_4$, DCE/*i*PrOH, 85°C.

Scheme 1. Synthesis of **SO4** and **SO5**.

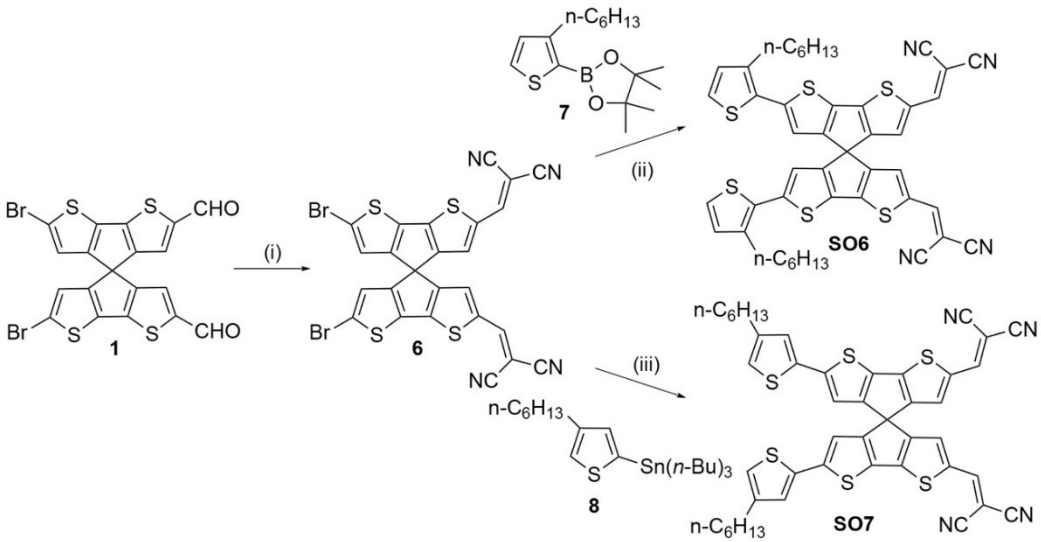

(i) $CH_2(CN)_2$, $Ti(OiPr)_4$, DCE/*i*PrOH, 85°C; (ii) $Pd(PPh_3)_4$, KF_{aq}, DME, 80°C; (iii) $PdCl_2(PPh_3)_2$, DMF, 65°C.

Scheme 2. Synthesis of **SO6** and **SO7**.

The cross-coupling/Knoevenagel sequence gave poor results in the case of monomer **SO6**. Indeed, the Pd-catalyzed reaction between **1** and 3-hexylthiophene-2-boronic acid pinacol ester **7** performed under various conditions failed to give the desired product in acceptable yields. We, therefore, decided to reverse the order of functionalization of the SCPDT core, introducing first the dicyanovinylene acceptor groups by Knoevenagel condensation of **1** with malononitrile in the presence of titanium tetraisopropoxide as Lewis acid catalyst (Scheme 2). The readily isolated intermediate **6** was then used as the precursor of monomers **SO6** and **SO7**. Suzuki-Miyaura cross-coupling of **6** with **7** afforded **SO6** in 34% yield, whereas

SO7 was isolated in 54% upon Stille cross-coupling of **6** with tributyl(4-hexyl-2-thienyl)stannane **8**.

Photophysical properties of SOs molecules. The steady-state absorption, emission, and excitation spectra of **SOs** in various aprotic solvents are shown in Figure 2 and the main optical transitions are reported in Table 1. DFT calculations were also performed to validate the interpretation of the experimental results (see later in the text and Supporting Information).

All the dyes spectra display three bands, two in the UV region, and a third much more intense band close to 500 nm.

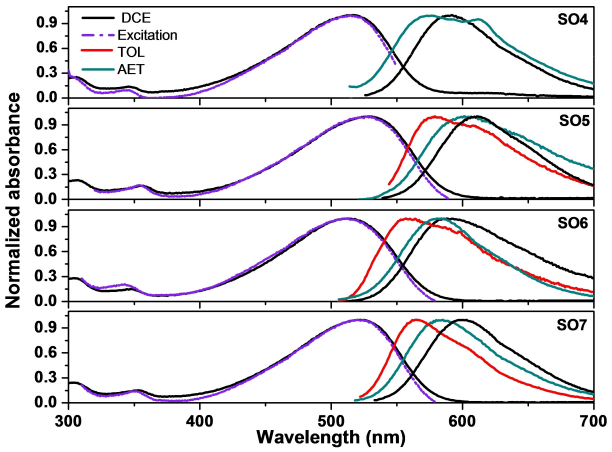

Figure 2. Normalized absorption and excitation spectra in solution of dichloroethane (DCE, black and violet line, respectively). Fluorescence spectra in DCE (black line), toluene (TOL, red line), and ethyl acetate (AET, green line)

Table 1. Optical and electrochemical properties of **SOs**.

	Abs. [nm]/ solvent[a]	Emiss. [nm]/ solvent[a]]	$E_{monomer}$ [V][b]	E_{film} [V][d]	HOMO [eV][e]	LUMO [eV][e]
SO4	307, 347, 516/DCE	590/DCE	0.72	0.30	−5.40	−3.17
	304, 348, 505/AET	576/AET				
SO5	306, 355, 526/DCE	610/DCE	0.68[c]	–	–	–
	294, 341, 501/AET	602/AET				
		579/TOL				
SO6	305, 349, 514/DCE	589/DCE	0.77	0.31	−5.41	−3.17
	303, 340, 496/AET	580/AET				
		558/TOL				
SO7	306, 352, 523/DCE	600/DCE	0.80	0.61	−5.71	−3.51
	301, 348, 508/AET	582/AET				
		564/TOL				

[a] Wavelength maxima values corresponding to UV-vis absorption and emission spectra of **SOs** in solution. The emission spectra were measured by excitation at the maximum wavelength of the lower energy absorption bands. [b] Peak potential of first oxidation wave. [c] Process-half-wave potentials. [d] Onset potentials of the electrodeposited films. [e]) Energy levels of **SOs** films obtained using the following equations: HOMO = −(E_{film} + 5.1), LUMO = −($E_{optical\ gap}$ − HOMO), and $E_{optical\ gap} = 1240/\lambda_{max.}$[48]

The bands around 300 nm and 350 nm can be associated with the π-π* electronic transitions in the conjugated backbone.[41] The higher extinction coefficient absorption band detected at longer wavelengths can be attributed to an intramolecular charge transfer (ICT) in the excited state from the electron-rich thiophenic part of the molecule to the dicyanovinylene acceptor unit, which is supported by the solvatochromism observed in the corresponding emission spectra.[41–43]

The **SOs** dyes shown in Figure 1 represent a structurally related homogeneous series where the length of conjugated systems in both branches bonded in a spiro configuration is fixed. **SO4** and **SO6** have their π-π* electronic transitions band at ~350 nm shifted approximately six nm to a higher energy than those belonging to **SO5** and **SO7** in DCE solution (see Table 1). The observed redshift is therefore possibly prompted by the steric effect exerted by the hexyl chain placed in the different positions of the pendant thiophene rings, which favors a higher degree of coplanarity between the thiophene and bithiophene units in **SO5** and **SO7** concerning **SO4** and **SO6**, thus affecting the π-π* transition energy The coplanarity between the dicyanovinylene unit and bithiophene bridge favors the photoinduced charge transfer and accounts for the high absorption intensity of the band.[41,43–46]

As observed for the π-π* electronic transitions at ~350 nm, slight differences in the grade of coplanarity between the thiophene and bithiophene moieties affect the ICT transition energy. Thus, in DCE solution **SO4** and **SO6** showed similar ICT light absorption maxima wavelengths at 516 nm and 514 nm, respectively, whereas maxima for **SO5** and **SO7** in the same solvent are about 10 nm red-shifted, being centered at 526 nm and 523 nm, respectively. Therefore, optical data indicate that the introduction of an *n*-hexyl chain in positions 4 or 5 of the pendant thiophene rings extends the **SO5** and **SO7** conjugation length compared to **SO6** where the steric interaction between the α-methylene of the alkyl chain in the 3-position and the nearest sulfur lone pair of the cyclopentadithiophene moiety results in some deviation from planarity. In the case of unsubstituted **SO4**, the observed blue-shift in absorbance in comparison to **SO5** and **SO7** can be ascribed to the inductive effect of the alkyl sidechains which is maximal in the terminal 5-position.[47]

On the other hand, all dyes show photo-stimulated light emission in aprotic solvents solution (Figure 2) where it is observed that the fluorescence band maxima have the same optical shifts pattern than the light absorption maxima. Dyes with the shortest length conjugation emit light at higher energy than the more conjugated dyes. Thus, **SO4** and **SO6** in DCE solution show emission at 590 nm and 589 nm, respectively, while **SO5** and **SO7** at around 600 nm (Figure 2 and Table 1). This behavior is in agreement with the previously discussed steric effect produced by the side alkyl chain. At the same time, the ICT character of the emission optical transition is manifested by a clear solvatochromic effect. **SOs** dyes emission maxima are strongly dependent on the solvent polarity. For example, when **SO6** in toluene solution is excited at ICT band wavelength, the emission band maximum appears at 558 nm, and upon increasing the solvent polarity the emission band is red-shifted

around 20 nm (AET)–30 nm (DCE) (Figure 2). Similar behavior is observed for **SO5** and **SO7** dyes, but in these cases, the change of polarity effect is more noticeable, with a redshift of ~40 nm switching the solvent from toluene to DCE (Table 1). **SO4** afforded poor quality emission spectra in toluene solution, possibly due to the presence of aggregates. Nevertheless, the batochromic shift can be evidenced by comparison of the emission band maxima in AET (576 nm) and DCM (590 nm). These results confirm the formation of a polarized excited state associated with an ICT process from the electron-donating thiophene rings to the electron-acceptor dicyanovinylene group. Again, the optical data show that the improved coplanarity between thiophene rings of **SO5** and **SO7** increases the conjugation length and now this effect manifests in increasing the ICT character, which indicates that there is some degree of electronic coupling between the pendant thiophene rings as electron donors and the dicyanovinylene groups as electron acceptors in the excited state.

In agreement, DFT calculations show that for all **SOs** monomers the highest occupied molecular orbital (HOMO) is principally localized on the thiophenic part of the molecule, and the lowest unoccupied molecular orbital (LUMO) on the dicyanovinylene residues (see Figure S1, Supporting Information). At the same time, the DFT optimized dihedral angle (θ_1) between pendant thiophene and the bithiophene bridge (see Figure 1), varies significantly with the position of the alkyl chain for the **SOs** monomers in their neutral state As shown in Table 2, the torsion angle calculated for **SO6** is 145.8°, while **SO5** and **SO7** reach a higher coplanarity, with torsion angles of 162.3° and 162.6°, respectively, close to the value calculated for **SO4**.

Electrochemical properties of SOs molecules. The electrochemical studies of **SOs** molecules were carried out with the aim to determine their redox properties, the stability of the electrochemically generated radical ions, and to evaluate their film growth capability by electrodeposition. These characteristics are eventually determined by the diverse substitution arrangements of the pendant thiophene rings attached to the perpendicularly aligned, independently behaving cyclopentadithiophene branches, as the **SOs** molecules differ from each other only in this respect.

For all molecules, the first potential scan of the multicyclic voltammograms (Figure 3, red lines) exhibits a similar oxidation wave close at 0.75 V. However, clear differences of electrochemical behavior emerge from the inspection of the appearance of the following successive potential scans.

Table 2. Selected stereoelectronic parameters for the DFT optimized geometries of **SOs** molecules and the corresponding radical cations.

	θ_1[a]	θ_1[b]	Spin Density[b] (C_α)	Charge Density[b] (C_β)
SO4	162.5°	179.1°	0.084	0.057
SO5	162.3°	178.7°	0.089	0.038
SO6	145.8°	160.3°	0.078	0.041
SO7	162.6°	177.1°	0.097	0.052

[a] Ground state. [b] Radical cation

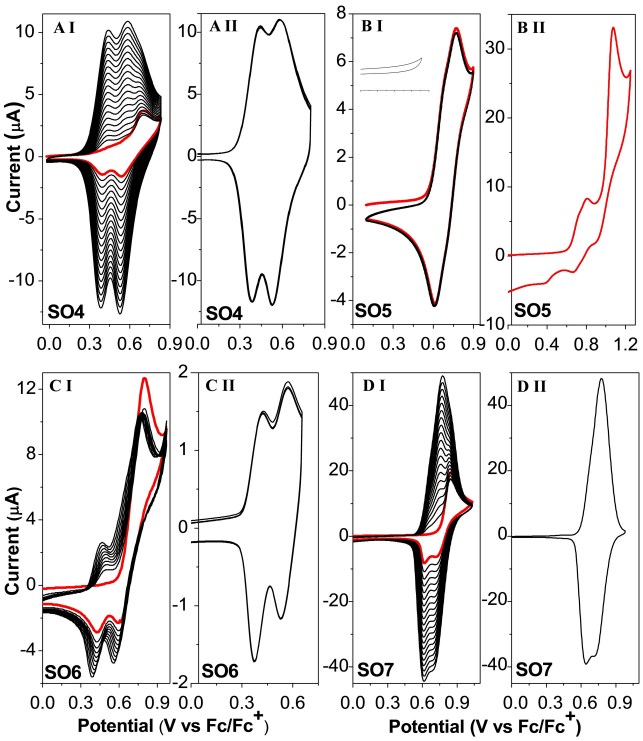

Figure 3. Multiple scan cyclic voltammogram of **SO4** A(I), **SO5** B(I and II), **SO6** C(I) and **SO7** D(I). Red line shows the first cycle for each monomer. The electrochemical response of the electrodeposited films are also shown (**SO4** = A(II), **SO6** = C(II) and **SO7** = D(II)). Inset **SO5** B(I): cyclic voltammetry on monomer-free electrolyte solution. (Conditions: Pt working electrode, electrolyte 0.1 M $TBAPF_6$/DCE, scan rate 0.1 V s^{-1}).

As shown in Figure 3 A(I), the **SO4** peak current at 0.69 V grows with the number of potential scans, while a new complementary peak system at ~0.4 V, which it absents in the first potential sweep, is detected. Such voltamperometric behavior is fully consistent with the occurrence of an electropolymerization process (exemplified in Scheme 3) happening via monoelectronic oxidation of the thiophene rings to give radical cations species, followed by their coupling to produce an oxidizable layer on the electrode, more easily oxidizable than the starting material due to the increased conjugation length.[4]

To evaluate the electrodeposited film formation and its redox behavior, once successive voltammetry cycles were finished, the working electrode was removed from the cell and immersed in a monomer-free support electrolyte solution, and then electrochemically tested. The **SO4** modified electrode redox response is shown in Figure 3 A(II), where two high reversibility oxidation processes with complementary peak maxima at 0.44/0.38 V and 0.59/0.53 V and a film onset potential of 0.30 V (Table 1) are observed.

Compared to **SO4**, the first cycle voltammogram of **SO5** (Figure 3 B(I), red line) shows the expected redox reversible process with maximum peak at 0.77 V and the complementary reduction wave in the cathodic sweep at 0.6 V. For both **SO4** and **SO5** each molecular branch consists of three linked thiophene units, and the loss of one electron leads to the

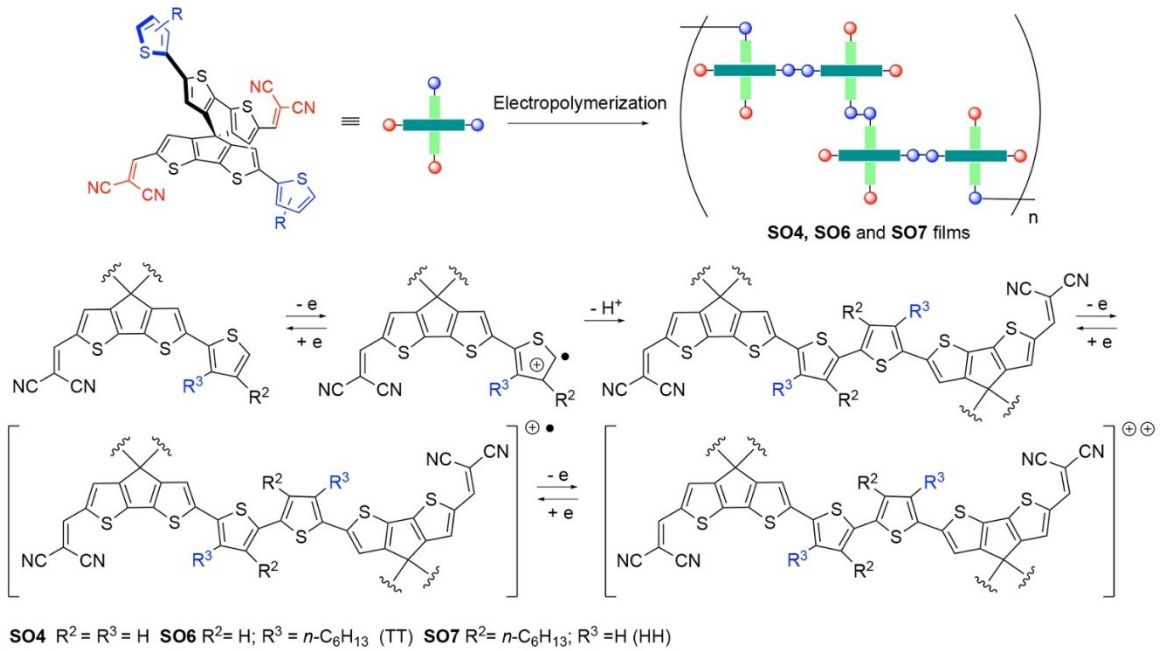

Scheme 3. Electrochemical oxidation and coupling modes for **SO4**, **SO6** and **SO7** monomers and oligomers.

corresponding cationic radical species. The observed different electrochemical behavior can be explained assuming that, contrary to **SO4**, the radical cation generated from **SO5** does not undergo coupling reactions that would produce thiophene chain elongation. As consequence, when the potential scan is continually cycled (Figure 3 B(I), black line), the observed current does not grow regarding the first swept, and no extra peak is detected at lower potentials, differently from what was observed for **SO4**. The inset in Figure 3 B(I) shows that the working electrode has not electrochemical signal in monomer-free support electrolyte solution after successive voltammetry cycles in **SO5** solution, which corroborates that no film is deposited on the electrode surface. On the other hand, when the potential is swept towards more positive values a second current wave appears, with irreversible electrochemical process characteristic (Figure 3 B(II)). Therefore, forcing a second electron abstraction only produce an unstable dication species centered on **SO5.**

The different electrochemical behavior of **SO4** and **SO5** is easily understood in the light of the well-known conduct of thiophene oligomers (three or more rings) with their terminal α-positions blocked with alkyl chains. These oligomers can be oxidized stepwise to form mono radical cation and dication species, the chemical stability of which depends on the number of linked thiophene units. For example, thiophene trimers can generate stable radical cation species, but their conjugation length is too short to ensure chemical stability to the dication, which can be reached when at least four thiophene ring units are present in the oligomer.[39,49,50] Thus, the repetitive coupling of **SO4** monomers through the pendant thiophene rings (Scheme 3) would produce oligomeric/polymeric chains of spiro-linked donor-acceptor repeat units, each comprising of two cyclopentadithiophene moieties joined by dithiophene for a total of six thiophene rings (without free terminal α-positions). The shown **SO4** film oxidation processes in Figure 3 A(II) are indicative of the stepwise stable generation of delocalized radical cation and dication species on these repeat units.

All these findings indicate that the electropolymerization process is effectively inhibited by the presence of *n*-C_6H_{13} chains in the α-positions of the pendant thiophene rings (see **SO5** molecular structure in Figure 1), in agreement with the reported electrochemical behavior of thiophene trimers with terminal α-alkyl groups.[49,50] The well-known predisposition of thiophene-based monomers and oligomers to form polymer chains dominantly or even exclusively through the bonding at unsubstituted α positions must be also considered.[39,49–51] Furthermore, the complete inhibition of electropolymerization processes for **SO5** strongly supports the notion that the SCPDT core and the dicyanovinylene terminal groups are not directly involved in the electrochemically driven formation of new bonds observed for the other **SOs** monomers, as also suggested by spin density calculations (vide infra).

In the case of **SO6** and **SO7** the pendant thiophene rings bear *n*-C_6H_{13} in their 3- and 4-positions, respectively (Figure 1), leaving the α position of each ring free for the electropolymerization process evidenced by their voltamperometric behavior. However, the different placement of the alkyl chain has a high impact on the electrochemical properties of the two isomers, as illustrated in Figure 3 C(I) and Figure 3D(I) showing the first voltamperometric cycles (red lines) and subsequent potential scan cycles (black lines), for **SO6** and **SO7**, respec-

tively. Under the same experimental conditions, the two dyes displayed noticeable differences in their capabilities to electrodeposit films. In particular, **SO6** presented a sluggish electric current growth between the different potential scanning cycles regarding the vigorous **SO7** current growth. The redox response of the resulting modified electrodes in a monomer-free electrolyte solution, shown in Figure 3 C(II) and Figure 3 D(II), is also markedly different, with the **SO7** film giving about twenty times larger oxidation current than the **SO6** film. This indicates that **SO7** produces a bigger amount of deposited electroactive material on the electrode surface than **SO6**. For the same reasons outlined in the case of **SO4**, the onset oxidation potentials of the thiophene-based polymeric films produced by **SO6** and **SO7** are lower than those of the corresponding monomers. However, the **SO7** film shows an onset oxidation potential of 0.61 V, which is ~300 mV higher than the ones measured for **SO4** and **SO6** films (Table 1), and a single anodic current peak instead of two

The analysis of the observed differences in film growth rate and material deposition efficiency with specific **SOs** molecular structures is far from being a trivial task. This is because the rate of electropolymerization of thiophene derivatives is simultaneously affected by several factors, such as stereoelectronic effects, solubility properties, lateral alkyl chains interactions that can affect the film conductivity, among others.[38,52] In this context, it is important to note that the rate of the initial coupling of radical cations generated from monomers has a major influence on the whole process. The overall rate of the electropolymerization process largely depends on the stability of these charged species, which is affected in turn by both the conjugation length and electron acceptor/donor substituents that modulate the thiophene ring electronic density and hence its reactivity. In particular, it is well-known that the unpaired electron spin density of thiophene-based radical cations is a good indicator of reactivity for the coupling reaction.[38,52] Therefore, the unpaired electron spin density distributions of **SOs** radical cations were determined by DFT calculations (Supporting Information, Tables S1-S4). The most relevant values are those pertaining to the α-positions of the pendant thiophene rings, which are reported in Table 2. In agreement with the observed electropolymerization rate tendency, **SO7** and **SO6** have the highest (0.097) and the lowest (0.078) spin densities at Cα of the oxidized thiophene rings, respectively, while **SO4** shows an intermediate value (0.084).

On the other hand, strongly electron-withdrawing substituents such as the dicyanovinylene groups present in the **SOs** molecules increase the oxidation potential of monomers and usually preclude the electropolymerization process. This has been attributed to the high reactivity of the radical cations that undergo rapid reactions with the solvent or other species (e.g. anions) to give soluble products, rather than to electropolymerize.[38]

In principle, **SO7** could be more susceptible than **SO6** to the effects of the dicyanovinylene groups. As pointed out above, **SO5** and **SO7** monomers have better coplanarity between thiophene rings and longer conjugation length than **SO6** (see Table 1 and Table 2), which is manifested in the ICT transition energy. Consequently, **SO7** mono radical cation is stabilized in a longer delocalization length, but this good ring coplanarity could boost the dicyanovinylene inductive effect on the α-position of the thiophene ring, resulting in a decrement of the spin density in this crucial position with respect to **SO6**. The adjacency of the alkyl chains to the α-position could also disfavor the radical cation coupling in the case of **SO7**, because of steric hindrance. Aside, it should be considered that the electronic effects exerted by the alkyl chains can affect the positive charge and spin density distributions on the atoms of the pendant thiophene ring.[38,52] Thus, an alkyl-chain in β-position of the thiophene ring allows locating the positive charge and the unpaired electron of the radical cation in the β-position and in the α-position, respectively.[52,53] In agreement, DFT calculations on radical cation species show that the positive charge density in the β-position of the pendant thiophene ring is higher for **SO7** with respect to **SO6** (Table 2). Therefore, compared to **SO6** the radical cation generated from **SO7** owns a more favorable positive charge and spin density distribution that facilitates the radical-radical coupling rate-determining step and justifies the observed ease of electrodeposition. Furthermore, the presence of *n*-hexyl chains increases the solubility of the **SO6** and **SO7** monomers and of their electrochemically formed oligomers regarding unsubstituted **SO4**. This factor, and the intermolecular interactions between the oligomeric units in the solid phase, could have a different incidence for the two alkyl-substituted materials, determining their different predisposition to precipitate on the electrode surface to form a film.

The picture emerging from the electrochemical experiments is summarized in Scheme 3. The electrochemically-driven oxidation of **SO4**, **SO6**, and **SO7** leads to the formation of mono radical cations with different capabilities of dimerization, which undergo regiospecific carbon-carbon coupling at the unsubstituted α-positions of the pendant thiophene rings, to produce dimeric species with conjugation length extended from three to six thiophene rings. The dimerization process occurs independently on the two perpendicularly aligned branches of the monomer, giving rise to 3D polymeric structures featuring spiro-linked donor-acceptor repeat subunits comprising of six bonded thiophene rings.

Positional isomerism of **SO6** and **SO7** monomers is reflected in the resulting polymers that differ for the configuration of the dialkyl-substituted dithiophene moieties generated in the coupling process. Thus, in each repeat unit of **SO6** and **SO7** polymers the relative orientation of the two *n*-C_6H_{13} chains corresponds to that observed in tail-to-tail (TT) and head-to-head (HH) coupled 3-alkylthiophenes, respectively, leading to a diverse degree of steric interference in the two polymers. This has obvious consequences; such has the dissimilar occurrence of twisted structures that affect the π-conjugation length along to the polymer chain. The presence and location of alkyl moieties in the hexathiophenic segment also influence intermolecular interactions, for example, π-stacking, lattice interactions, swelling, among others.[38,54] Altogether, these features can modulate the morphological order and functional proper-

ties of the **SOs** polymeric films, as proved by subsequent analysis.

Surface and Spectroelectrochemical Characterization of the Electrogenerated Films. The morphological and electro-optical characteristics of electrogenerated **SOs** thin films deposited on a transparent semiconductor electrode (ITO) were next investigated. In the case of **SO6**, the above-mentioned low electropolymerization capability of the monomer impeded to obtain good quality films. Therefore, the study was restricted to **SO4** and **SO7**.

Morphology of the conducting film is a key factor in determining the stability and performance of organic optoelectronic devices, as the presence of defects, cracks and/or roughness on the film favors short circuits or current passages with different resistances. The morphological characterization of the **SOs** electrochemically deposited films in their neutral form was thus performed by SEM. The images obtained for **SO4** and **SO7** on ITO electrodes are shown in Figure 4.

The surface morphologies of the two polymers films were quite similar despite the clear differences observed in the growth cyclic voltammograms discussed above and shown in Figure 3. The polymer structures completely cover the ITO electrodes, without cracks, pinholes, or leaving unfilled spaces. Therefore, electrochemical deposition conditions provide an adequate surface morphology to be used in the manufacture of optoelectronic devices. The granulated surfaces evidenced by the images in Figure 4 are typical of electrodeposited films.[55–58] However, the grain size seems to be somewhat different, with better defined and larger size grains in the case of the **SO7** film. It has been reported that there is a correspondence between this kind of morphology and the conductive properties, which would position **SO7** as the most conductive film.[55]

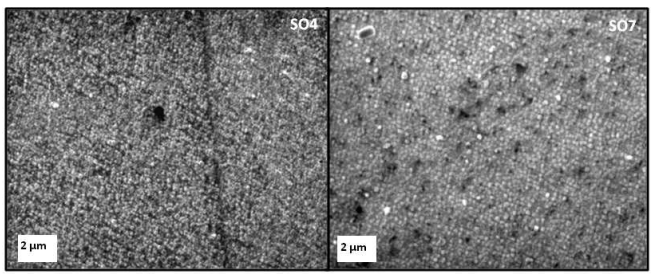

Figure 4. SEM micrographs of **SO4** (left) and **SO7** (right) films with 135 nm and 183 nm of thickness respectively.

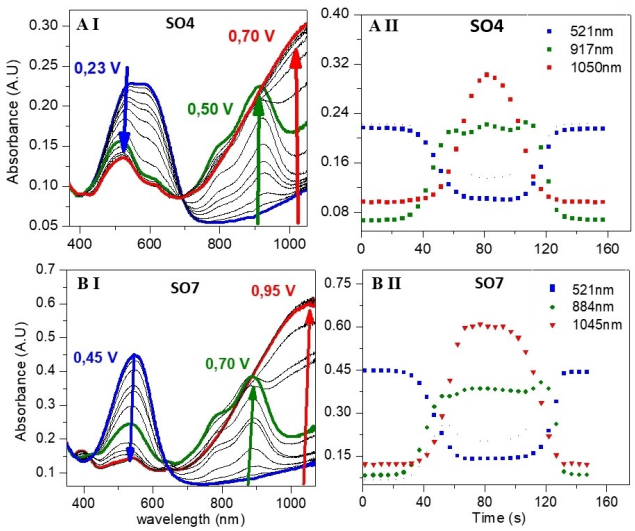

Figure 5. Absorption spectra of **SO4** (A) and **SO7** (B) electrodeposited films as a function of applied potential in electrolyte solution 0.1 M TBAPF6/DCE, scan rate 0.050 V s^{-1} (pictures **I**, left side). On the right side (pictures **II**): traces of light absorbed by the electrodeposited films as a function of time at the wavelengths indicated by arrows.

Figure 5 shows the optical spectra of **SO4** and **SO7** films in the neutral (blue lines) and oxidized states, which can be compared with the absorption spectra of the corresponding monomers reported in Figure 2.

For both polymers, an intense absorption band with a maximum at ~520 nm was observed in the neutral state (Figure 5, A(I) and B(I)), indicating that the ICT transition observed in the corresponding monomers is retained. However, the spectrum of **SO4** film exhibits a shoulder at lower energy close to 605 nm (Figure 5, A(I)), which is neither present in the corresponding monomer spectrum (Figure 2 and Table 1), nor in the spectrum of **SO7** film (Figure 5, B(I)). This low energy optical transition points to an increment of conjugation length in **SO4** regarding **SO7** electroformed materials. On the other hand, the absorption spectra of **SO4** and **SO7** films are responsive to the increase of applied potential and the subsequent generation of oxidized species. First, the ICT band intensity decreases, while concomitantly new optical transitions loom up (see arrows in Figure 5A(I) and Figure 5B(I)): when the applied potential attains 0.50 V (**SO4**) and 0.70 V (**SO7**), the new optical transitions detected at 917 nm (**SO4**) and 884 nm (**SO7**) reach their maxima. Then, when the bias potential exceeds 0.70 V and 0.95 V for **SO4** and **SO7**, respectively, similar light absorption broadband with a maximum above 1000 nm is observed for both polymer films.

Figures 5A(II) and Figure 5B(II) show the traces absorption vs. time for the main spectroelectrochemical processes occurring in **SO4** and **SO7** films, respectively. It is evident that for both materials the ICT band at 521 nm decreases as the bias potentials applied increase, reaching a minimum when the films are fully oxidized. At the same time, the trace assigned to the oxidized species at ~900 nm and above of 1000 nm reach a complementary maximum; when the potential scan is switched in the inverse direction, all traces go back to their original light absorption values, which indicates good reversibility of the **SOs** films redox processes.

The new optical transitions at 917 nm and 884 nm can be attributed to mono radical cation species, and the longer absorption wavelength observed in the case of **SO4** clearly indicates a higher charge delocalization degree with respect to **SO7**. Furthermore, the formation of **SO4** radical cations at lower potential (0.5 V) than **SO7** (0.7 V) is in good agreement with the films' onset potential reported in Table 1, where **SO7** film shows an onset potential 300 mV higher than **SO4**. Vacuum DFT calculations performed on **SO4** and **SO7** homodimers corrobo-

rate the hypothesis that the effective conjugation length of the hexathiophenic repeat unit (Figure 6) in oligo/polymeric species is affected by steric hindrance. Thus, for **SO7** minimization of steric interactions between the alkyl chains on the central dithiophene moiety results in a pronounced thiophene-thiophene twist angle ($\theta_2 = -114.8$) that interferes with the extension of the conjugation length beyond three thiophene rings regarding **SO4** (Table 3 and Figures S2–S4 in Supporting information).

Although a good agreement is found between the DFT optimized geometries of **SOs** homodimers and the observed optical and electrochemical properties, it should be pointed out that the optoelectric properties of regioregular polymer film are also affected by solid-state packing induced by the side saturated hydrocarbon chains and the interaction with the solvent. The analysis of these aspects is beyond the scope of this study, but it remains an important exercise for future research.

Conclusion

The spiro-configured bis-cyclopentadithiophene scaffold was functionalized to give electropolymerizable electron-donor acceptor monomers **SOs** that served as precursors for the preparation of thin films of polymers featuring cylopentadithiophene-dithiophene-cylopentadithiophene repeat units connected through spiro carbon atoms. Thanks to the chemical information embedded in the monomeric structures, uniform polymer backbone arrangements were obtained without resort to the demanding synthetic strategies previously applied to achieve the regiospecific insertion of the cylopentadithiophene-dithiophene motif in polymeric chains.[59]

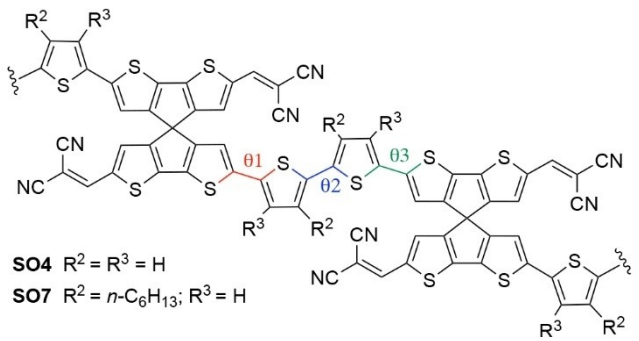

Figure 6. Repeat unit in **SOs** polymers.

Table 3. Selected torsion angles for the DFT optimized geometries of **SOs** homodimers and the corresponding radical cations.

	θ_1[a]	θ_2[a]	θ_3[a]	θ_1[b]	θ_2[b]	θ_3[b]
SO4	164.1°	169.4°	164.1°	179.9°	179.9°	179.9°
SO7	154.8°	−114.8°	154.8°	165.4°	−132.7°	165.4°

[a] Ground state. [b] Radical cation.

The electrochemical and photophysical properties of the **SOs** monomers, which differ from each other for the presence and/or location of an additional *n*-hexyl chain on one of their pendant thiophene units, were investigated, as well as their susceptibility to electrochemical polymerization. The substitution arrangement of the monomers was found to exert significant influence on the outcome of the electropolymerization process, on the optoelectronic properties, and morphological film characteristics of the new regioregular materials obtained. The results obtained provide a firm ground for the design of more elaborated regioregular electropolymers with applications in optoelectronic devices.

Experimental Section

Synthesis of monomers: All available reagents were purchased from commercial sources and were used without any further purification. Solvents were purified by standard methods and dried if necessary. Tributyl(4-hexyl-2-thienyl)stannane **8** were prepared as described in the literature.[60] Reactions were monitored by thin-layer chromatography (TLC) that was conducted on plates precoated with silica gel Si 60-F254 (Merck, Germany). Column chromatography was carried out on silica gel SI 60 (Merck, Germany), mesh size 0.063–0.200 mm (gravimetric) or 0.040–0.063 mm (flash). Melting points were determined with a capillary melting point apparatus Büchi B-540. ^{1}H NMR and ^{13}C NMR were recorded on a Bruker Avance 400 spectrometer (400 and 100.6 MHz, respectively). ESI and EI mass spectra were obtained with a LCQ Fleet ion trap mass spectrometer (Thermo Fisher) and a VG AUTOSPEC- M246 spectrometer (double-focusing magnetic sector instrument with EBE geometry), respectively.

2,2′-Diformyl-6,6′-bis-(2-thienyl)-4,4′-spirobi[cyclopenta[2,1-*b*:3,4-*b*′]dithiophene] (3): A flame-dried Schlenk tube was charged with **1** (110 mg, 0.19 mmol), 2-thienylboronic acid **2** (108 mg, 0.84 mmol), tetrakis(triphenylphosphine)palladium (45 mg, 0.04 mmol) and dry 1,2-dimethoxyethane (10 mL), evacuated, and backfilled with nitrogen twice. After the addition of an aqueous solution of KF (2.76 M, 0.5 mL, 1.38 mmol), the mixture was stirred at 85 °C for 20 h. After cooling, the mixture was treated with water and diluted with CH_2Cl_2. The aqueous phase was extracted with CH_2Cl_2 and the combined organic phase was washed with water, brine and dried over $MgSO_4$. After removal of the solvent at reduced pressure, the residue was purified by flash column chromatography (silica gel, CH_2Cl_2/hexane/AcOEt 45/50/5) affording the title compound (76 mg, 68 % yield) as an orange solid. M.p. > 250 °C (dec.). ^{1}H-NMR($CDCl_3$): $\delta = 9.71$ (s, 2H), 7.25–7.22 (m, 4H), 7.20 (dd, $J_1 = 1.1$ Hz, $J_2 = 3.6$ Hz 2H), 7.01 (dd, $J_1 = 3.6$ Hz, $J_2 = 5.1$ Hz 2H), 6.69 (s, 2H). ^{13}C-NMR ($CDCl_3$): $\delta = 182.4$, 153.9, 149.3, 148.9, 144.6, 143.6, 136.8, 136.4, 129.8, 128.3, 125.9, 124.6, 117.8, 57.9. IR (film) ν (cm^{-1}): 3108, 3063, 2920, 1649, 1494, 1425, 1395, 1310, 1223, 1145, 835, 697. MS (ESI): *m/z* calcd. for $C_{27}H_{12}O_2S_6$ $[M]^+$: 560.75, found 560.89.

2,2′-Bis-(2,2-dicyanovinyl)-6,6′-bis(2-thienyl)-4,4′-spirobi[cyclopenta[2,1-*b*:3,4-*b*′]dithiophene] (SO4): In a two-necked round bottom flask equipped with a reflux condenser and magnetic stirrer compound **3** (153 mg, 0.27 mmol) was dissolved in dry CH_2Cl_2 (20 mL). After the addition of malononitrile (72 mg, 1.08 mmol) and piperidine (5 µL, 0.05 mmol) the mixture was refluxed under stirring overnight. After cooling, the solvent was removed at reduced pressure and the residue was boiled with ethanol (3 mL) for 30 min. The mixture was cooled to room temperature and filtered on a Hirsch funnel. The solid residue was

washed with cold ethanol and dried under vacuum to give the title compound (53 mg, 30%) as a dark red solid, poorly soluble in organic solvents. TM.p. > 250 °C (dec.). ^{1}H-NMR(DMSO-d_6): δ = 8.32 (s, 2H), 7.55 (dd, J_1 = 5.0 Hz, J_2 = 1.0 Hz, 2H), 7.43 (dd, J_1 = 3.6 Hz, J_2 = 1.0 Hz, 2H), 7.39 (s, 2H), 7.08–7.06 (m, 4H). IR (KBr) ν (cm^{-1}): 2217, 1561, 1482, 1400, 1298, 1172, 1137, 839, 710. HRMS (EI): *m/z* calcd. for $C_{33}H_{12}N_4S_6$ [M]$^+$: 655.93863, found 655.93983.

2,2′-Diformyl-6,6′-bis(5-*n*–hexyl-2-thienyl)-4,4′-spirobi[cyclopenta[2,1-*b*:3,4-*b*′]dithiophene] (5): A flame-dried Schlenk tube was charged with **1** (51 mg, 0.092 mmol) and tetrakis(triphenylphosphine)palladium (27 mg, 0.023 mmol), evacuated, and backfilled with nitrogen twice. After the addition of dry 1,2-dimethoxyethane (4.4 mL), 5-hexylthiophene-2-boronic acid pinacol ester **4** (110 μL, 0.36 mmol) was added, followed by an aqueous solution of KF (2.76 M, 0.36 mL, 0.99 mmol). The mixture was stirred at 80 °C for 20 h. After cooling, the mixture was treated with water and diluted with CH_2Cl_2. The aqueous phase was extracted with CH_2Cl_2 and the combined organic phase was washed with water, brine and dried over $MgSO_4$. After the removal of solvent at reduced pressure, the residue was purified by flash column chromatography (silica gel, pentane/AcOEt 85/15) affording the title compound (43 mg, 65% yield) as a yellow glass. ^{1}H-NMR ($CDCl_3$): δ = 9.69 (s, 2H), 7.22 (s, 2H), 7.00 (d, J = 3.6 Hz, 2H), 6.67 (d, J = 3.6 Hz, 2H), 6.59 (s, 2H), 2.76 (t, J = 7.5 Hz, 4H), 1.69–1.58 (m, 4H), 1.42–1.16 (m, 12H), 0.94–0.82 (m, 6H). ^{13}C-NMR ($CDCl_3$): δ = 182.3, 154.1, 149.5, 148.7, 147.2, 144.3, 144.2, 135.6, 134.1, 129.8, 125.3, 124.4, 117.0, 57.8, 31.6, 31.6, 30.3, 28.8, 22.7, 14.20. IR (film) ν (cm^{-1}): 2959, 2924, 2852, 1656, 1496, 1397, 1261, 1140, 1098, 1020, 799. MS (EI): *m/z* calcd. for $C_{39}H_{35}O_2S_6$ [M–H]$^+$: 727.10, found 727.09.

2,2′-Bis-(dicyanovinyl)-6,6′-bis(5-*n*–hexyl-2-thienyl)-4,4′-spirobi[cyclopenta[2,1-*b*:3,4-*b*′]dithiophene] (SO5): A flame-dried Schlenk tube was charged with **5** (90 mg, 0.12 mmol), malononitrile (49 mg, 0.74 mmol), and dry dichloroethane (2 mL) under inert atmosphere. After the addition of 2-propanol (0.80 mL, HPLC grade) and Ti(OiPr)$_4$ (73 μL, 0.25 mmol) the mixture was heated at 80 °C under stirring overnight. The mixture was then cooled to room temperature and treated with HCl (10% aqueous solution, 2 mL). After 10 min. stirring, the mixture was diluted with CH_2Cl_2 and the organic phase was washed with saturated aqueous $NaHCO_3$, brine and dried over $MgSO_4$. After removal of the solvent at reduced pressure, the residue was washed with ethanol and after filtration the title compound (85 mg, 86% yield) was obtained as a purple solid. M.p. > 250 °C (dec.). ^{1}H-NMR($CDCl_3$): δ = 7.59 (s, 2H), 7.13 (s, 2H), 7.06 (d, J = 3.6 Hz, 2H), 6.69 (d, J = 3.6 Hz, 2H), 6.58 (s, 2H), 2.77 (t, J = 7.5 Hz, 4H), 1.7–1.5 (m, 4H), 1.4–1.2 (m, 12H), 0.9–0.8 (m, 6H). ^{13}C-NMR ($CDCl_3$): δ = 155.4, 152.6, 150.0, 149.2, 148.3, 146.9, 136.3, 135.2, 133.7, 130.8, 125.6, 125.2, 116.8, 114.7, 114.2, 73.6, 57.2, 31.6, 31.5, 30.4, 28.748, 22.7, 14.2. IR (KBr) ν (cm^{-1}): 2959, 2925, 2853, 2218, 1565, 1479, 1403, 1310, 1260, 1172, 1138, 1094, 1019, 801. HRMS (EI): m/z calcd. for $C_{45}H_{36}N_4S_6$ [M]$^+$: 824.12643, found 824.12701.

2,2′-Dibromo-6,6′-bis-(2,2-dicyanovinyl)-4,4′-spirobi[cyclopenta[2,1-*b*:3,4-*b*′] dithiophene] (6): A flame-dried Schlenk tube was charged with **1** (104 mg, 0.19 mmol), malononitrile (47 mg, 0.71 mmol), and dry dichloroethane (3.2 mL) under inert atmosphere. After the addition of 2-propanol (1.2 mL, HPLC grade) and Ti(OiPr)$_4$ (110 μL, 0.37 mmol) the mixture was heated at 75 °C under stirring overnight. The mixture was then cooled to room temperature and treated with HCl (10% aqueous solution, 4 mL). After 10 min. stirring, the mixture was diluted with CH_2Cl_2 to dissolve the solid. The organic phase was washed with water and brine and dried over $MgSO_4$. After removal of the solvent at reduced pressure, the residue was purified by flash column chromatography (silica gel, CH_2Cl_2) affording the title compound (105 mg, 86% yield) as an orange solid. M.p. > 250 °C (dec.). ^{1}H-NMR ($CDCl_3$): δ = 7.61 (s, 2H), 7.15 (s, 2H), 6.64 (s, 2H). ^{13}C NMR (101 MHz, $CDCl_3$) δ = 152.4, 151.1, 150.2, 148.5, 138.2, 136.9, 130.5, 124.6, 120.4, 114.2, 113.8, 75.6. IR (film) ν (cm^{-1}): 2219, 1564, 1490, 1416, 1384, 1307, 1183. MS (ESI): *m/z* calcd. for $C_{25}H_6Br_2N_4S_4$ [M]$^+$: 650.40, found 651.11.

2,2′-Bis-(dicyanovinyl)-6,6′-bis(3-*n*–hexyl-2-thienyl)-4,4′-spirobi[cyclopenta[2,1-*b*:3,4-*b*′]dithiophene] (SO6): A flame-dried Schlenk tube was charged with **6** (46 mg, 0.072 mmol) and tetrakis(triphenylphosphine)palladium (16.6 mg, 0.014 mmol, 20 mol%), evacuated, and backfilled with nitrogen twice. After the addition of dry 1,2-dimethoxyethane (4 mL), 3-hexylthiophene-2-boronic acid pinacol ester **7** (85 μL, 0.28 mmol) and an aqueous solution of KF (2.64 M, 0.25 mL, 0.66 mmol), the mixture was stirred at 80 °C for 17 h and then cooled to room temperature. The solvent was removed under reduced pressure and the residue taken up in CH_2Cl_2. The organic phase was washed with water and dried over $MgSO_4$. After the removal of the solvent under vacuum, the residue was purified by flash column chromatography (silica gel, hexane/CH_2Cl_2, from 40/60 to 20/80) affording the title compound (20 mg, 34% yield) as a dark solid. M.p. > 250 °C (dec.). ^{1}H-NMR ($CDCl_3$): δ = 7.60 (s, 2H), 7.34–7.10 (m, 6H), 6.93 (d, J = 5.3 Hz, 2H), 6.63 (s, 2H), 2.76 (t, J = 7.9 Hz, 4H), 1.70–1.50 (m, 4H), 1.40–1.30 (m, 12H), 0.95–0.8 (m, 6H). ^{13}C-NMR ($CDCl_3$): ^{13}C NMR (101 MHz, $CDCl_3$) δ = 154.7, 152.4, 150.1, 149.4, 145.4, 141.5, 136.8, 136.5, 130.8, 129.9, 125.6, 119.4, 114.6, 114.1, 74.0, 57.3, 31.7, 30.6, 29.8, 29.4, 22.8, 14.2. IR (KBr) ν (cm^{-1}): 2925, 2855, 2214, 1562, 1480, 1400, 1299. HRMS (EI): *m/z* calcd. for $C_{45}H_{36}N_4S_6$ [M]$^+$: 824.12643, found 824.12651.

2,2′-Bis-(dicyanovinyl)-6,6′-bis(4-*n*–hexyl-2-thienyl)-4,4′-spirobi[cyclopenta[2,1-*b*:3,4-*b*′]dithiophene] (SO7): A flame-dried Schlenk tube was charged with **4** (77 mg, 0.12 mmol) and dichlorobis(triphenylphosphine) palladium (5.2 mg, 0.0074 mmol), evacuated, and backfilled with nitrogen twice. After the addition of a solution of tributyl(4-hexyl-2-thienyl)stannane **8** (160 mg, 0.35 mmol) in dry DMF (2 mL), the mixture was heated at 65 °C and kept at this temperature under stirring overnight. After cooling, the mixture was treated with an aqueous solution of KF (1 M, 2 mL), stirred for 30 min and then diluted with CH_2Cl_2. After phase separation, the aqueous phase was extracted with CH_2Cl_2. The combined organic phase was washed with brine, dried over $MgSO_4$, filtered and evaporated under reduced pressure. The crude material was purified by flash chromatography (CH_2Cl_2/hexane 9/1) affording the title compound (54 mg, 54% yield) as a dark solid. M.p. > 250 °C (dec.). ^{1}H-NMR($CDCl_3$): δ = 7.60 (s, 2H), 7.14 (s, 2H), 7.07 (d, *J* = 1.3, 2H), 6.87 (d, *J* = 1.3, 2H), 6.64 (s, 2H), 2.56 (t, *J* = 7.6, 4H), 1.58 (q, *J* = 7.0, 4H), 1.37–1.23 (m, 12H), 0.94–0.80 (m, 6H). ^{13}C NMR (101 MHz, $CDCl_3$) δ = 155.2, 152.4, 150.0, 149.2, 146.7, 144.9, 136.5, 135.9, 135.6, 130.8, 126.6, 121.5, 117.3, 114.6, 114.1, 73.9, 57.2, 31.8, 30.5, 30.5, 29.0, 22.7, 14.2. IR (film) ν (cm^{-1}): 2924, 2213, 1561, 1480, 1400, 1298. HRMS (EI): *m/z* calcd. for $C_{45}H_{36}N_4S_6$ [M]$^+$: 824.12643, found 824.12701.

Photophysical characterization: UV-visible spectra were obtained using an Agilent HP 8453 multidiode spectrophotometer. Fluorescence spectra in solution were obtained with a SPEX Fluoromax Instruments spectrophotometer, using quartz cells NSG Precision Cell 10 mm optical path. The measurements were done in solvents of different polarity 1,2-dichloroethane (DCE), toluene (TOL), and ethyl acetate (AET).

Electrochemical and photoelectrochemical characterization: The electrochemical measurements of the redox properties of the molecules under study, as well as the generation of electropolymers, were carried out with a CHI6208E electrochemical analyzer using of a conventional three-electrode cell. Two types of

working electrodes were used: Pt disc of 2.16×10^{-3} cm^2 area and indium tin oxide (ITO) (Delta Technologies, nominal resistance of strength 70–100 Ω/square). A silver wire quasi-reference electrode was used. Voltammetric experiments were performed in a deoxygenated solution (nitrogen bubbling for 15–20 minutes) of DCE, with 0.10 M tetra-*n*-butylammonium hexafluorophosphate ($TBAPF_6$) as the supporting electrolyte. The Pt working electrode was cleaned between experiments by polishing with 0.3 μm alumina paste followed by solvent rinses. After each voltammetric experiment, ferrocene was added as an internal standard, and the potential axis was calibrated against for the normal hydrogen electrode ($Fc^+/Fc = 0.70$ V vs NHE).[48] Details of DFT calculations on **SOs** monomers and dimers are reported in the Supporting Information.

Film surface analysis. The topographic analysis of the surfaces of the electrodes covered by the electropolymer was performed by scanning electron microscopy (SEM). For this, a Carl Zeiss EVO MA 10 microscope with a 3 KV electron beam was used. The samples were analyzed without prior treatment.

Acknowledgements

We are grateful to Secretaría de Ciencia y Técnica de la Universidad Nacional de Río Cuarto (SECYT-UNRC), Ministerio de Ciencia y Tecnología – Gobierno de Córdoba for financial support. D.M., G.M., P.C., L.F. and F.F are scientific members of CONICET. S.O, M.C., S.R., and G.P. are indebted to Prof. Cozzi for his enthusiastic teaching, and a lot of fun.

Conflict of Interest

The authors declare no conflict of interest.

Keywords: Cyclic voltammetry · Density functional calculations · Spiro compounds · Sulphur heterocycles · Thin films

[1] S. Sharma, S. Shriwastava, S. Kumar, K. Bhatt, C. Charu Tripathi, *Opto-Electron. Rev.* **2018**, *26*, 223–235.
[2] T. P. I. Saragi, T. Spehr, A. Siebert, T. Fuhrmann-Lieker, J. Salbeck, *Chem. Rev.* **2007**, *107*, 1011–1065.
[3] F. Fungo, K.-T. Wong, S.-Y. Ku, Y.-Y. Hung, A. J. Bard, *J. Phys. Chem. B* **2005**, *109*, 3984–3989.
[4] J. Londenberg, T. P. I. Saragi, I. Suske, J. Salbeck, *Adv. Mater.* **2007**, *19*, 4049–4053.
[5] X.-D. Zhu, X.-J. Ma, Y.-K. Wang, Y. Li, C.-H. Gao, Z.-K. Wang, Z.-Q. Jiang, L.-S. Liao, *Adv. Funct. Mater.* **2019**, *29*, 1807094.
[6] D. Heredia, L. Fernandez, L. Otero, M. Ichikawa, C.-Y. Lin, Y.-L. Liao, S.-A. Wang, K.-T. Wong, F. Fungo, *Phys. Chem. C* **2011**, *115*, 21907–21914.
[7] F. M. Sawatzki, D. H. Doan, H. Kleemann, M. Liero, A. Glitzky, T. Koprucki, K. Leo, *Phys. Rev. Appl.* **2018**, *10*, 034069.
[8] *Organic Lasers: Fundamentals, Developments, and Applications* (Eds.: M. Anni, S. Lattante), Pan Stanford Publishing, Singapore, **2018**.
[9] K. Gao, B. Xu, C. Hong, X. Shi, H. Liu, X. Li, L. Xie, A. K.-Y. Jen, *Adv. Energy Mater.* **2018**, *8*, 1800809.
[10] B. Zhang, Y. Xu, J. Yang, Y. Liao, L. Tong, S. Zhou, *Comput. Theor. Chem.* **2019**, *1166*, 112575.
[11] D. Heredia, J. Natera, M. Gervaldo, L. Otero, F. Fungo, C.-Y. Lin, K.-T. Wong, *Org. Lett.* **2010**, *12*, 12–15.
[12] B. B. Carbas, A. M. Önal, *Electrochim. Acta* **2012**, *66*, 38–44.
[13] D. Vak, J. Jo, J. Ghim, C. Chun, B. Lim, A. J. Heeger, D. Y. Kim, *Macromolecules* **2006**, *39*, 6433–6439.
[14] L.-H. Xie, F. Liu, C. Tang, X.-Y. Hou, Y.-R. Hua, Q.-L. Fan, W. Huang, *Org. Lett.* **2006**, *8*, 2787–2790.
[15] H.-F. Chen, T.-C- Wang, W.-Y. Hung, H.-C. Chiu, C. Yun, K.-T. Wong, *J. Mater. Chem.* **2012**, *22*, 9658–9664.
[16] M. Saliba, S. Orlandi, T. Matsui, S. Aghazada, M. Cavazzini, J. P. Correa-Baena, P. Gao, R. Scopelliti, E. Mosconi, K. H. Dahmen, F. De Angelis, A. Abate, A. Hagfeldt, G. Pozzi, M. Grätzel, M. K. Nazeeruddin, *Nat. Energy* **2016**, *1*, 15017.
[17] S. Ma, H. Zhang, N. Zhao, Y. Cheng, M. Wang, Y. Shen, G. Tu, *J. Mater. Chem. A* **2015**, *3*, 12139–12144.
[18] N. Arora, S. Orlandi, M. I. Dar, S. Aghazada, G. Jacopin, M. Cavazzini, E. Mosconi, P. Gratia, F. De Angelis, G. Pozzi, M. Grätzel, M. K. Nazeeruddin, *ACS Energy Lett.* **2016**, *1*, 107–112.
[19] R. Nakar, F. J. Ramos, C. Dalinot, P. S. Marques, C. Cabanetos, P. Leriche, L. Sanguinet, M. Kobeissi, P. Blanchard, J. Faure-Vincent, F. Tran-Van, N. Berton, J. Rousset, B. Schmaltz, *J. Phys. Chem. C* **2019**, *123*, 22767–22774.
[20] N. Harindu Hemasiri, S. Kazim, L. Calio, S. Paek, M. Salado, G. Pozzi, L. Lezama, M. K. Nazeeruddin, S. Ahmad, *ACS Appl. Mater. Interfaces* **2020**, *12*, 9395–9403.
[21] M. Li, S. Tang, F. Shen, M. Liu, W. Xie, H. Xia, L. Liu, L. Tian, Z. Xie, F. Lu, M. Hanif, D. Lu, G. Cheng, Y. Ma, *J. Phys. Chem. B* **2006**, *110*, 17784–17789.
[22] S.-S. Kim, S.-I. Na, S.-J. Kang, D.-Y. Kim, *Sol. Energy Mater. Sol. Cells* **2010**, *94*, 171–175.
[23] F. C. Krebs, *Sol. Energy Mater. Sol. Cells* **2009**, *93*, 465–475.
[24] F. C. Krebs, *Sol. Energy Mater. Sol. Cells* **2009**, *93*, 394–412.
[25] M. C. Petty in *Encyclopedia of Nanoscience and Nanotechnology* (Ed.: H. S. Nalwa), American Scientific Publishers, Valencia (USA), **2004**, pp. 295–304.
[26] A. Palma-Cando, U. Scherf, *Macromol. Chem. Phys.* **2016**, *217*, 827–841.
[27] L. Otero, L. Sereno, F. Fungo, Y.-L. Liao, C.-Y. Lin, K.-T. Wong, *Chem. Mater.* **2006**, *18*, 3495–3502.
[28] P. Zabel, T. Dittrich, Y.-L Liao, C.-Y Lin, K.-T. Wong, F. Fungo, L. Fernandez, L. Otero, *Org. Electron.* **2009**, *10*, 1307–1313.
[29] Y.-S. Su, T.-Y. Wu, *Polymer* **2017**, *9*, 284.
[30] S. Orlandi, G. Pozzi, M. Cavazzini, D. Minudri, M. Gervaldo, L. Otero, F. Fungo, *Macromolecules* **2015**, *48*, 4364–4372.
[31] V. Jeux, C. Dalinot, C. M. Allain, L. Sanguinet, P. Leriche, *Tetrahedron Lett.* **2015**, *56*, 1383–1387.
[32] G. Pozzi, S. Orlandi, M. Cavazzini, D. Minudri, L. Macor, L. Otero, F. Fungo, *Org. Lett.* **2013**, *18*, 4642–4645.
[33] T. K. Das, S. Prusty, *Polym.-Plast. Technol. Eng.* **2012**, *51*, 1487–1500.
[34] X. Lv, W. Li, M. Ouyang, Y. Zhang, D. S. Wright, C. Zhang, *J. Mater. Chem. C* **2017**, *5*, 12–28.
[35] G. Zotti, G. Schiavon, A. Berlin, G. Fontana, G. Pagani, *Macromolecules* **1994**, *27*, 1938–1942.
[36] M. Horie, L. A. Majewski, M. J. Fearn, C.-Y. Yu, Y. Luo, A. Song, B. R. Saunders, M. L. Turner, *J. Mater. Chem.* **2010**, *20*, 4347–4355.
[37] B. P. Cherniawski, S. A. Lopez, E. K. Burnett, I. Yavuz, L. Zhang, S. R. Parkin, K. N. Houk, A. L. Briseno, *J. Mater. Chem. C* **2017**, *5*, 582–588.
[38] J. Roncali, *Chem. Rev.* **1992**, *92*, 711–738.
[39] A. B. Nepomnyashchii, R. J. Ono, D. M. Lyons, C. W. Bielawski, J. L. Sessler, A. J. Bard, *Chem. Sci.* **2012**, *3*, 2628–2638.
[40] G. Bidan, A. De Nicola, V. Enée, S. Guillerez, *Chem. Mater.* **1998**, *10*, 1052–1058.
[41] P. Sun, H. Sun, X. Li, Y. Wang, H. Shan, J. Xu, C. Zhang, Z. Xu, Z. K. Chen, W. Huang, *Dyes Pigm.* **2017**, *139*, 412–419.
[42] M. Caselli, D. Vanossi, M. Buffagni, M. Imperato, L. Pigani, A. Mucci, F. Parenti, *ChemPlusChem* **2019**, *84*, 1314–1323.
[43] R. Fitzner, E. Reinold, A. Mishra, E. Mena-Osteritz, P. Bäuerle, H. Ziehlke, C. Körner, K. Leo, M. Riede, M. Weil, O. Tsaryova, A. Weiß, C. Uhrich, M. Pfeiffer, *Adv. Funct. Mater.* **2011**, *21*, 897–910.
[44] M. M. Bader, P. T. T. Pham, E. H. Elandaloussi, *Cryst. Growth Des.* **2010**, *10*, 5027–5030.
[45] L. Zhang, N. S. Colella, B. P. Cherniawski, S. C. B. Mannsfeld, A. L. Briseno, *ACS Appl. Mater. Interfaces* **2014**, *6*, 5327–5343.
[46] A. Wadsworth, M. Moser, A. Marks, M. S. Little, N. Gasparini, C. J. Brabec, D. Baran, I. McCulloch, *Chem. Soc. Rev.* **2019**, *48*, 1596–1625.
[47] C. J. Lee, F. M. Jradi, V. D. Mitchell, J. White, C. R. McNeill, J. Subbiah, S. Marder, D. J. Jones, *J. Mater. Chem. C* **2020**, *8*, 567–580.
[48] C. M. Cardona, W. Li, A. E. Kaifer, D. Stockdale, G. C. Bazan, *Adv. Mater.* **2011**, 23, 2367–2371.

[49] J. Guay, P. Kasai, A. Diaz, R. Wu, J. M. Tour, L. H. Dao, *Chem. Mater.*, **1992**, *4*, 1097–1105.
[50] J. Guay, A. Diaz, R. Wu, J. M. Tour, *J. Am. Chem. Soc.* **1993**, *115*, 1869–1874.
[51] Y. Wei, C. C. Chan, J. Tian, J. G. W. Jang, K. F. Hsueh, *Chem. Mater.* **1991**, *3*, 888–897.
[52] S. Ando, M. Ueda, *Synth. Met.* **2002**, *129*, 207–213.
[53] A. Smie, A. Synowczyk, J. Heinze, R. Alle, P. Tschuncky, G. Götz, P Bäuerle, *J. Electroanal. Chem.* **1998**, *452*, 87–95.
[54] I. Osaka, R. D. McCullough, *Acc. Chem. Res.* **2008**, ***41***, 1202–1214.
[55] M. I. Mangione, R. A. Spanevello, D. Minudri, D. Heredia, L. Fernandez, L. Otero, F. Fungo, *Electrochim. Acta* **2016**, *207*, 143–151.
[56] M. Grzeszczuk, R. Ozsakarya, *RSC Adv.* **2014**, *4*, 22214–22223.
[57] M. Gervaldo, M. Funes, J. Durantini, L. Fernandez, F. Fungo, L. Otero, *Electrochim. Acta* **2010**, *55*, 1948–1957.
[58] I. Pecnikaj, S. Orlandi, G. Pozzi, M. V. Cappellari, G. Marzari, L. Fernandez, M. A. Zensich, L. Hernandez, F. Fungo, *Langmuir* **2019**, *35*, 8732–8740.
[59] S. W. Chang, T. Muto, T. Kondo, M. J. Liao, M. Horie, *Polym. J.* **2017**, *49*, 113–122.
[60] H.-H. Cho, T. E. Kang, K.-H. Kim, H. Kang, H. J. Kim, B. J. Kim, *Macromolecules* **2012**, *45*, 6415–6423.

Manuscript received: November 12, 2020
Revised manuscript received: November 19, 2020
Accepted manuscript online: November 20, 2020